

Article

Challenges in Contacting Metal–Polymer Current Collectors in Pouch Cells

Hakon Gruhn *¹, Tobias Krüger, Malte Mund, Maja W. Kandula and Klaus Dilger 

Institute of Joining and Welding, TU Braunschweig, Langer Kamp 8, 38106 Braunschweig, Germany

* Correspondence: h.gruhn@tu-braunschweig.de

Abstract: Recent research focuses on replacing metal current collectors with metallized polymer foils. However, this introduces significant challenges during cell production, as manufacturing steps must be adapted. Currently, copper is used as the current collector on the anode side and aluminum on the cathode side. These current collectors are then joined within the cell with an arrester tab. This step, known as contacting, is carried out industrially in pouch cells using ultrasonic welding or laser beam welding. However, since the polymer foil is electrically insulating, the current contacting procedures cannot be directly transferred to the metal–polymer current collectors. In this work, ultrasonic welding, laser beam welding, and a mechanical contacting method are considered, and the challenges arising from the material properties are highlighted. The properties of the joints are discussed as a function of the number of foils and the coating thickness of the metallization. It is demonstrated that successful contacting by ultrasonic welding and mechanical clamping is possible, as both mechanical strength and electrical conductivity are ensured by the joint. Laser beam welding was unsuccessful. Additionally, the electrical resistance is one to two orders of magnitude higher than that of pure aluminum and copper foils, which necessitates further optimization. Furthermore, ultrasonic welding is limited to welding 16 foils or fewer. This does not match industrial requirements. Consequently, novel approaches for contacting metal–polymer current collectors are required.



Citation: Gruhn, H.; Krüger, T.; Mund, M.; Kandula, M.W.; Dilger, K. Challenges in Contacting Metal–Polymer Current Collectors in Pouch Cells. *J. Manuf. Mater. Process.* **2023**, *7*, 219. <https://doi.org/10.3390/jmmp7060219>

Academic Editor: Dulce Maria Rodrigues

Received: 13 November 2023

Revised: 1 December 2023

Accepted: 4 December 2023

Published: 5 December 2023



Copyright: © 2023 by the authors. Licensee MDPI, Basel, Switzerland. This article is an open access article distributed under the terms and conditions of the Creative Commons Attribution (CC BY) license (<https://creativecommons.org/licenses/by/4.0/>).

Keywords: contacting; joining; welding; metal–polymer current collector; laser beam welding; clamping

1. Introduction

A lithium-ion battery is typically composed of anodes and cathodes. These electrodes both consist of an active material coating deposited on a current collector. For electrochemical reasons, aluminum foil is used for the cathode, while copper foil is employed on the anode side [1,2]. The current collectors fulfill two primary functions: firstly, they serve as a substrate for the active material coating, and secondly, they conduct electrons out of the cell [3,4]. Therefore, it is essential that the stacked electrodes be contacted, i.e., joined, with an arrester tab. This process is referred to as internal contacting [3,5–7]. Two properties of the joint are crucial in this context. On the one hand, sufficient mechanical strength must be ensured [8]. On the other hand, it is imperative that the electrical resistance of the joint be as low as possible, as this directly correlates with the power dissipation and heat generation in the cell via Joule heating [9]. In pouch cells, ultrasonic (US) metal welding or laser beam welding is primarily employed to join the copper and aluminum foils, as both methods are capable of welding a large number of electrodes [2,8,10]. The resulting electrical resistances are well below one milliohm [11].

However, current research endeavors are focused on replacing the metallic current collectors with thermoplastic polymer foils that are metallized on both sides [12]. The metallization consists of aluminum for the cathodes and copper for the anodes. A primary reason for the substitution of the all-metal foils is the reduced amount of metal required, as the deposited metal layers are quite thin, about 0.5 µm to 1.0 µm [13–15]. This results in material savings, weight reduction, and an increase in the energy density of the cell [16].

However, the principal motivation for employing metal–polymer current collectors is the safety advantage provided by the thermoplastic polymer substrate. This substrate is designed to melt in the event of an internal short circuit within the cell due to the heat generated. This disrupts the electrical conduction path created by the short circuit and prevents the catastrophic failure of the cells by halting the thermal runaway of the cell (see Figure 1) [17,18].

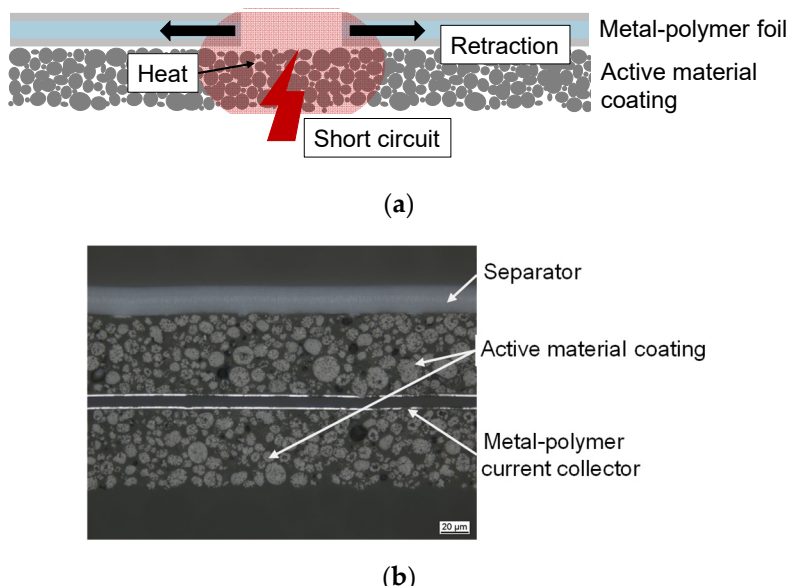


Figure 1. (a) Principle of metal–polymer current collectors (inspired by [17]) and (b) metal–polymer current collector in a laminated cathode.

But, the implementation of these innovative collectors is not without its challenges. A significant disadvantage of polymer-based current collectors is the potential inapplicability of conventional welding processes due to the temperature sensitivity of the foils. Therefore, transferring the processes to the novel polymer-based current collectors is challenging due to the electrically insulating thermoplastic core [19]. Despite the insulating substrate, the welding processes must ensure sufficient electrical conductivity [20]. Ideas to achieve this by welding on metal foils or modifying the current collectors are already patented [21–24]. However, to date, there have been no publications addressing the realization and the resulting joint properties of contacting metal–polymer current collectors.

The feasibility of welding thin plastic foils or fibers to metal foils using laser transmission welding or local heating has been demonstrated in other application areas [25–27]. However, this requires transparency for the corresponding laser wavelength and direct contact between the polymer and metal. This is not the case with metal–polymer current collectors.

Ultrasonic plastic welding of polymers and composite materials with metals has also been investigated [28]. This welding process has been successfully implemented [29]. Similar to the welding of two thermoplastics, the oscillation at the interface between metal and polymer causes the parts to be joined to heat up and the polymer to melt, resulting in a direct connection without the need for additives [30]. Direct contact between the thermoplastic of the first and the surface of the second joining part is a prerequisite here as well.

Extensive investigations, particularly at the chair of Heinz Palkowski at TU Clausthal, have been conducted in the field of metal–polymer–metal sheets for automotive engineering applications [31]. These sheets share a similar general structure with metal–polymer current collectors but differ in terms of materials and, most notably, thickness. They are intended for use in the car body. For this reason, the joinability was also considered, and laser welding proved to be suitable. The partial melting of the cover sheets was achieved without degrading the polymer core. The thickness of the cover sheets, 0.49 mm, ensures

sufficient heat dissipation, and the molten pool does not reach the polymer substrate [32]. Nonetheless, a direct transfer to metal–polymer current collectors is likely to be difficult.

The lack of previous publications on the joinability and the resulting properties of (multilayer) metal–polymer current collectors or similar materials necessitates a fundamental consideration. Therefore, this work investigates the suitability of laser beam and metal ultrasonic (US) welding as well as an alternative contacting method for joining the novel metal–polymer current collectors by clamping. The suitability of the joining processes was investigated and the weldability was evaluated. Furthermore, electrical resistance measurements and mechanical tests were performed and evaluated as a function of the number of welded foils, coating thickness, and polymer substrate. The classification of the joint properties is carried out by comparing them to each other and to the properties of welds with full metal foil.

2. Materials and Methods

2.1. Materials

The polymer substrate foils used in this study are commercially available biaxially oriented polyethylene terephthalate (PET) as well as polyethylene naphthalate (PEN) foils with thicknesses of 8 µm (Al@PET), 12 µm (Cu@PET), and 6 µm (Cu@PEN), respectively. These foils were metallized with high-purity aluminum as a current collector for cathodes and copper as a current collector for anodes in a roll-to-roll process via electron beam evaporation at Fraunhofer FEP (Dresden, Germany). Within this coating process, different thicknesses of the metals were deposited. An overview of the produced foils is given in Table 1.

Table 1. Overview of the investigated metal–polymer current collectors with its sheet resistance in milliohm per square ($\text{m}\Omega/\square$).

Variant	Polymer Substrate	Coating	Sheet Resistance
V1	8 µm PET	1050 nm Aluminum	Approx. 40 $\text{m}\Omega/\square$
V2	12 µm PET	Copper (varying thickness)	241–24.1 $\text{m}\Omega/\square$
V3	6 µm PEN	Copper (varying thickness)	217–40.6 $\text{m}\Omega/\square$

2.2. Manufacturing of the Specimens

Three different joining techniques were utilized to contact the metallized foils. Besides two welding processes, a mechanical clamping process was implemented. To produce the specimens, the metallized polymer foils were cut into $100 \times 20 \text{ mm}^2$ strips. Then, a defined number of the stripes were stacked and finally joined using ultrasonic welding, laser beam welding, or mechanical clamping.

Ultrasonic welding was performed with a Branson L20 ultrasonic metal welder (Danbury, CT, USA). The welding area was $11 \times 7 \text{ mm}^2$. The knurling of the horn was pyramidal with an edge length of 1.0 mm. The foils were welded to an arrester tab with a width of 10 mm and a length of 52 mm. The tabs were made of aluminum for the aluminum-metallized foils and nickel-plated copper for the copper-metallized foils. The thickness of the tabs was 0.2 mm in all cases. The arrester tab was placed on top of the foils to prevent adhesion of the metal–polymer current collector foils to the horn. A schematic representation of the materials to be welded and the location of the weld area is shown in Figure 2.

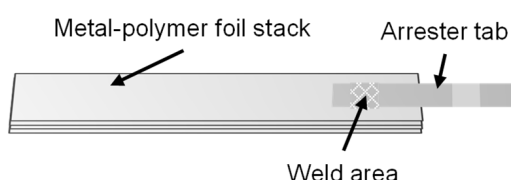


Figure 2. Concept of ultrasonically welded specimen.

For laser beam welding experiments, a TruPulse 2020 nano laser from Trumpf (Ditzingen, Germany) was used to join the foils. The laser had an average maximum power of 200 W and a spot diameter of 70 μm . For the laser beam welding studies, waveform 0 was set with a pulse frequency of 200 kHz, resulting in a pulse length of 261 nm. The beam has a Gaussian shape with an M^2 of 1.3 and a wavelength of 1064 nm.

The focus for laser welding was set on the surface of the foil stack. For this purpose, 10 foils were clamped together with an arrester tab underneath to achieve a zero gap, as shown in Figure 3. The weld length was set to be 10 mm at a scan speed of 10 mm/s. An AXIALSCAN-30-Y scanner (RAYLASE AG, Wessling, Germany) was used for this purpose. The laser power was varied between 10 W and 200 W. REMARK: It should be noted that it is not possible to achieve a welded joint due to the material properties of the metal–polymer current collectors (further details in Section 3.2).

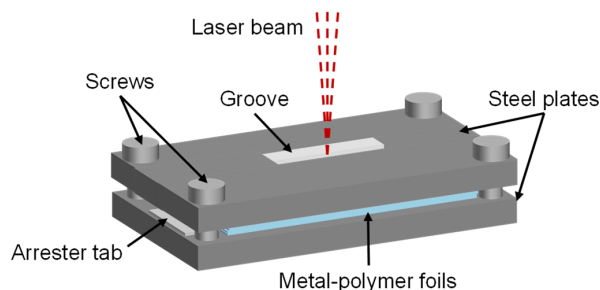


Figure 3. Clamps for laser beam welding to achieve a zero gap.

As an alternative joining method to welding, joining based on mechanical clamping was considered. To contact the foils, a special arrester tab was designed. It consists of an upper and a lower part. The metal–polymer current collectors were positioned between the clamped parts. Both parts of the clamp are shown in Figure 4. The material used was 300 μm aluminum.

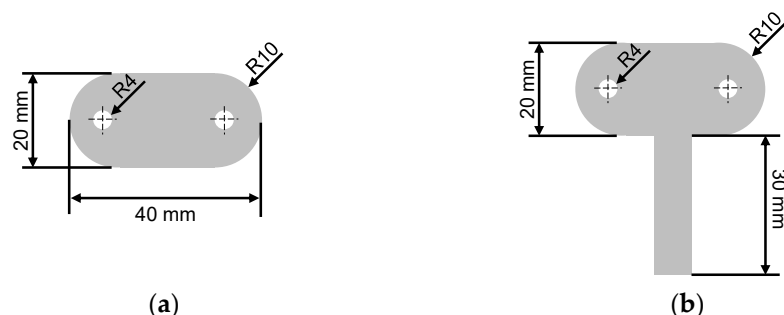


Figure 4. (a) Contact aids and top, respectively, (b) bottom arrester tab design for mechanical clamping.

However, since the clamp could not contact all of the foils, 20 μm aluminum contact aids were alternatively stacked with the metal–polymer current collectors. Clamping was performed using two M4 stainless steel bolts and nuts with a torque of 3 Nm. The resulting joint is illustrated in Figure 5.

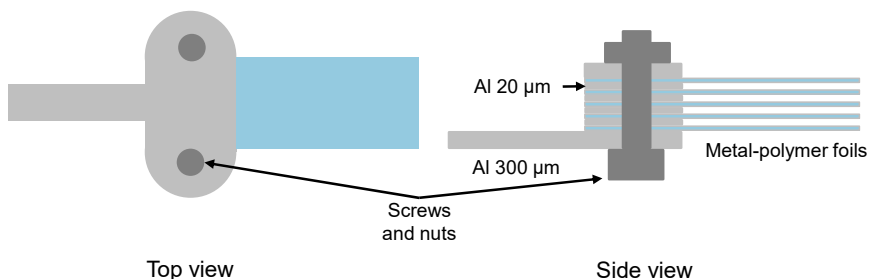


Figure 5. Specimen buildup for mechanical contacting by clamping.

2.3. Testing Methods

2.3.1. Evaluation of the Joint Characteristics Using Non-Destructive Testing

One of the primary challenges in evaluating the ultrasonic welding process is the limited access for in situ measurement. Due to the sample being covered by the anvil and horn during the welding process, as well as the low total thickness of the specimens, optical in situ measurement is not practical. Consequently, efforts are focused on measuring vibration amplitude, such as using laser vibrometers in research, to control the welding process [33]. The relative movement of the tools could serve as a termination criterion [34]. However, there is insufficient data on this, especially for multilayer specimens. Therefore, the current industrial state of the art is to monitor the process using the system's internal parameters (e.g., power) [35]. While this is suitable to ensure process stability, it provides limited information about the resulting weld properties, even for common full metal sheets [35–37].

Consequently, all joints were subjected to non-destructive testing after welding. This involved a visual assessment according to Figure 6. Three distinct cases were identified. Under-welding (a) resulted in welds with insufficient adhesion or a lack of fusion within the foil stack or between the foils and the arrester tab. These welds could be distinguished from properly welded joints (b). Additionally, damaged foils (c) could be identified when over-welding occurred, which was often accompanied by the sticking of the joint to the anvil.

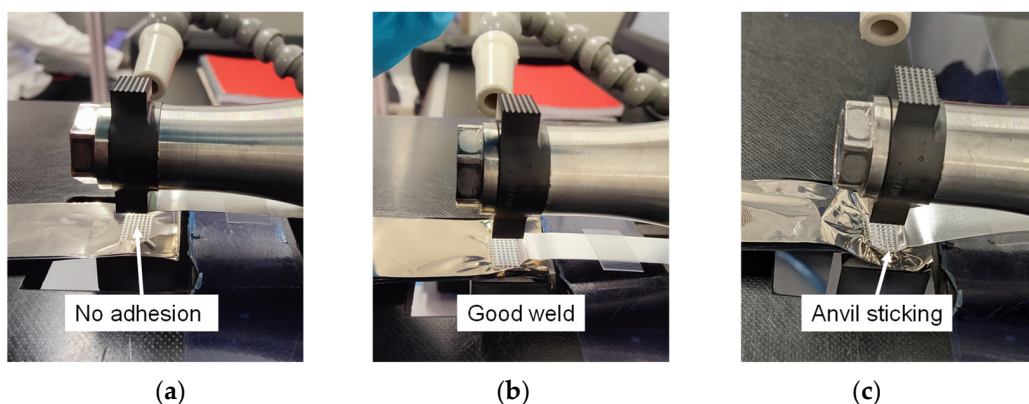


Figure 6. Visual assessment of ultrasonically welded joints: (a) no joint achieved (under weld), (b) good joint achieved/good weld, and (c) anvil sticking and damage of foils (over weld).

In addition, computed tomography (CT) scans were taken to evaluate the internal structure of the welds. This enabled the detection of internal defects such as wrinkles and cracks. A computed tomography system (phoenix v|tome|x s 240 microCT) from GE Sensing & Inspection Technologies GmbH (Wunstorf, Germany) was used for this purpose.

2.3.2. Mechanical Testing of the Specimens

To determine the mechanical properties, tensile tests were conducted using a zwickiLine universal tensile testing machine equipped with a 1 kN load cell (ZwickRoell GmbH & Co. KG, Ulm, Germany). The specimens were clamped in rubberized grips at a distance of 60 mm on the arrester tab and foil stack and tested at a rate of 2 mm/min. The maximum force recorded was used as the result value, referred to as the fracture force.

2.3.3. Electrical Resistance Measurement

To measure the electrical resistance of the joints (weld resistance), four-point probe measurements were conducted using a Resistomat 2329 from Burster GmbH & Co. KG (Gernsbach, Germany). The inner probes were positioned one millimeter from the joint on the foil or tab to measure the voltage potential. The outer probes were placed 6 mm away from the inner probes (see Figure 7). The electrical resistance was then calculated as the quotient of the voltage difference between the inner probes and the current flowing through

the outer probes. This method eliminates the influence of lead and contact resistances. The resolution was $10 \mu\Omega$.

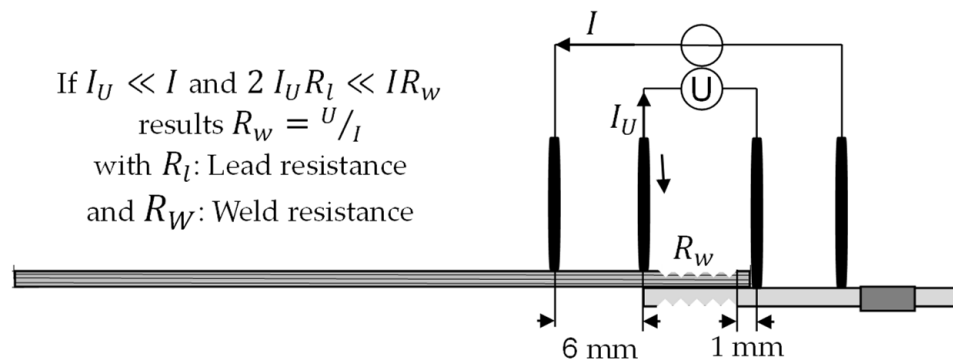


Figure 7. Four-point probe measuring principle for electrical resistance measurement on ultrasonically welded specimens.

3. Results

The weld characteristics of the laser-beam-welded, US-welded, and clamped specimens are shown below. In addition, the weldability as a function of welding parameters, coating thickness, polymer substrate, and number of foils welded is addressed.

3.1. Ultrasonic Welding

To investigate the weldability of metal–polymer current collectors by ultrasonic welding, a parameter study was conducted and the welded specimens were examined through visual inspection, CT scans, and electrical resistance measurements. During the study, the welding parameters of energy, force, and amplitude were varied to determine their influence on the welding process and the welded joint.

Figure 8 presents exemplary CT scans of three different welds produced with different welding parameter sets, resulting in visually acceptable welds. The welded stack consists of 10 aluminum-coated PET foils (V1) and a 20 μm aluminum foil as an arrester tab.

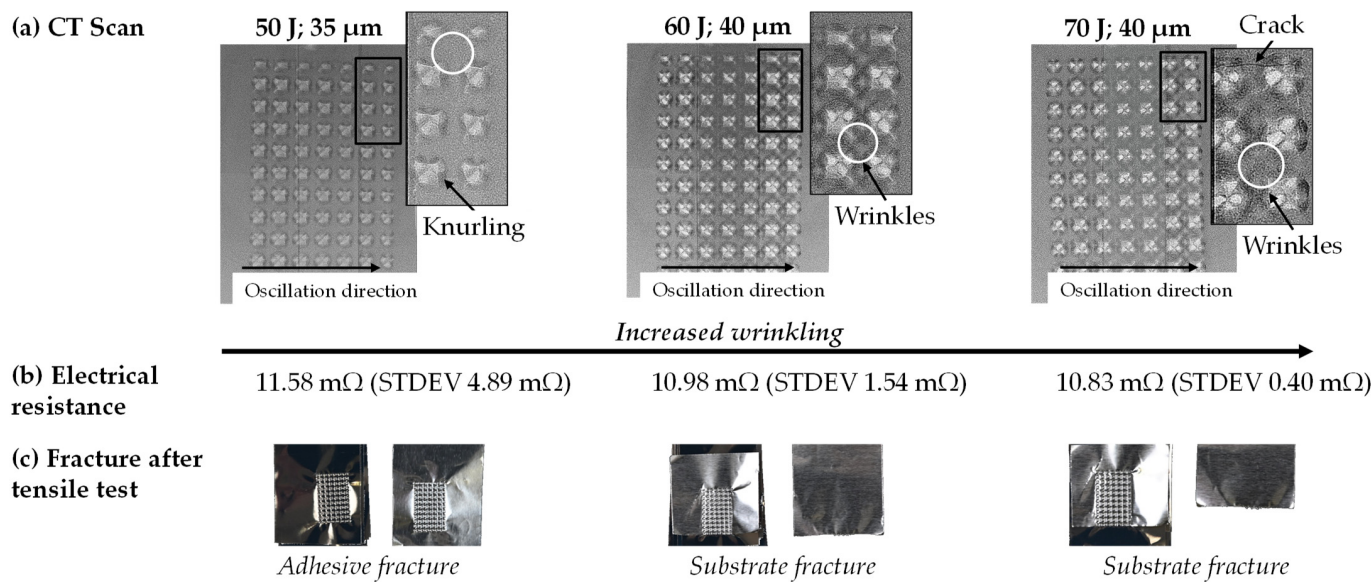


Figure 8. Dependence of the weld quality on the ultrasonic welding parameters: (a) CT scans of the welds, (b) electrical resistances of the specimens, and (c) fracture patterns after tensile tests.

The first specimen represents the specimen that was welded with the lowest energy input required to produce an acceptable joint. Consequently, it fractures via adhesive

fracture (at 15 N fracture force). To produce this specimen, a welding energy of 50 J, a welding amplitude 35 μm , and a welding pressure force of 1.1 kN were applied. The second set of specimens was joined with medium (60 J; 40 μm ; 1.1 kN), and the third with high (70 J; 40 μm ; 1.1 kN) energy input. In the case of the third specimen, strong adhesion of the specimen to the anvil was already observed.

The CT images of the specimens reveal that, with increasing welding energy and amplitude, the wrinkles between the horn tips increase sharply until cracks appear in individual foils at the maximum welding parameters. However, the four-point measurements show only minor differences in electrical resistance (Figure 8b), with a tendency toward slightly decreasing resistances and lower standard deviations with increasing welding parameters. The fracture pattern of the tensile tests show that adhesive fracture occurs for the specimens that were welded with the lowest energy input. In contrast, a substrate fracture appears when the energy input is increased. In the subsequent examinations, the welding parameters were always optimized for substrate fracture without over-welding taking place.

To assess the influence of the coating thickness on the weld properties, four of the metal–polymer current collectors were joined with a 200 μm tab. The foils used were coated with copper on both sides. Copper coating thicknesses between 125 nm and 1000 nm were considered. A 12 μm PET (V2) was used as the polymer substrate. The results of the mechanical tests as well as the resistance measurements are presented in Figure 9.

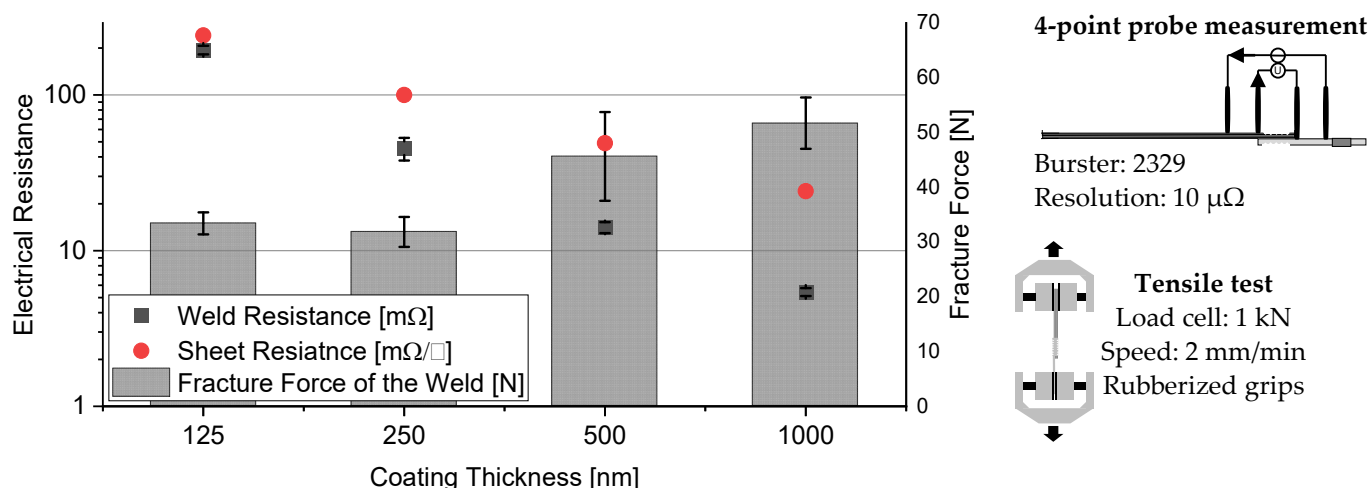


Figure 9. Mechanical and electrical properties of ultrasonically welded metal–polymer current collectors in dependence of the coating thickness resp. sheet resistance (in $\text{m}\Omega/\square$).

The results of the tensile tests show the strength of the welds increases as the coating thickness increases. Since substrate fracture occurred in all specimens, this is likely attributed to the enhanced load-carrying capacity and strength provided by the additional copper coating. The gain in fracture strength average 55% between the 125 nm and 1000 nm coating thicknesses. It is at least 33.4 N for the copper-coated PET foil, which is still sufficient for the mechanical loads within the cell.

Simultaneously, there is a linearly decreasing trend in sheet resistance as the copper coating thickness increases. Conversely, the electrical resistance of the welded joint decreases exponentially from an initial value of about 195 $\text{m}\Omega$ at a coating thickness of 125 nm to 5.4 $\text{m}\Omega$ at a coating thickness of 1000 nm. Thus, the electrical resistance of the weld correlates exponentially with the sheet resistance. Since the lowest weld resistance was recorded for the foils with the lowest sheet resistance and, therefore, the highest coating thickness, it can be concluded that higher coating thicknesses are favorable for contacting with ultrasonic welding.

As an alternative polymer substrate, a 6 μm PEN foil (V3) was also coated on both sides, welded to the arrester tab, and compared with the metallized PET substrate. The

comparison of weld resistances and sheet resistances for two coating thicknesses is given in Figure 10.

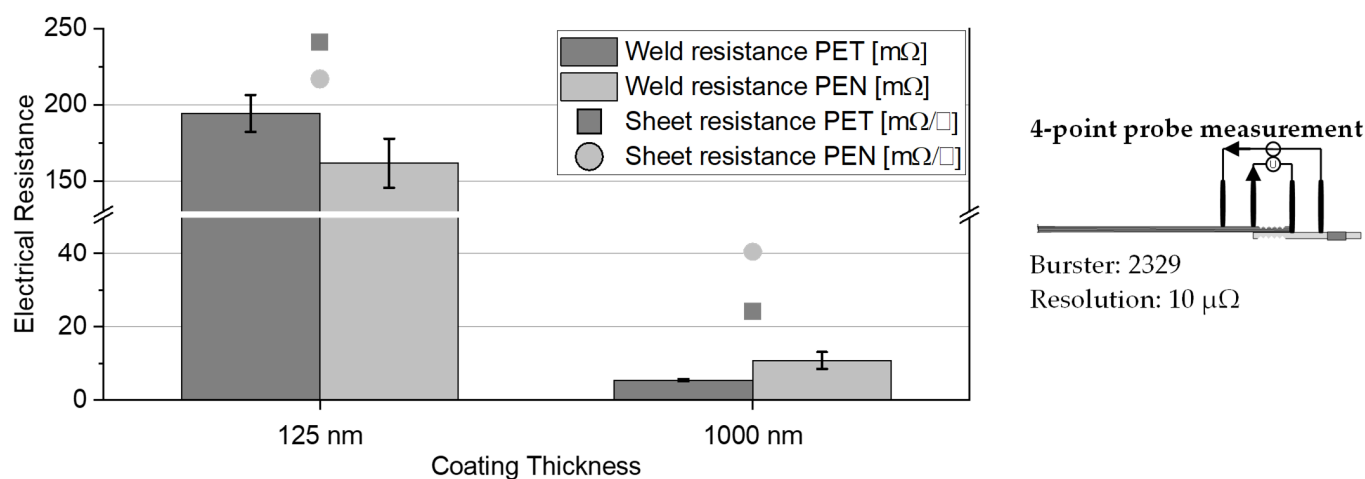


Figure 10. Comparison of metallized foils with different substrate materials and coating thicknesses resp. sheet resistances (in $\text{m}\Omega/\square$) in respect of the weld resistance (in $\text{m}\Omega$) after ultrasonic welding.

The diagram demonstrates that the sheet resistances of the two different polymer substrate materials differ at the same coating thickness (e.g., $24.1 \text{ m}\Omega/\square$ vs. $40.6 \text{ m}\Omega/\square$ at 1000 nm coating thickness). However, the weld resistances also vary and mirror this trend with resistances of $5.4 \text{ m}\Omega$ and $10.8 \text{ m}\Omega$, respectively. This trend is also evident in the measurements for the lower coating thickness of 125 nm . Considering this, the two substrates exhibit similar behavior. Therefore, it can be concluded that changes in weld resistance are reflected in the changes in sheet resistance. Since the substrate material does not influence the sheet resistance, it can be assumed that slight variations in the morphology or actual thickness of the copper coatings between the polymer substrates are present that have not been detected. Given this, no differences between the two substrates can be identified regarding the weld properties.

For pouch cell contacting, it is important to investigate how many foils can be welded and to what extent the joint properties change with the number of welded foils. To investigate these effects, the V1 foil with an aluminum coating thickness of 1050 nm was chosen, as it was also used in the sensitivity studies of the welding process. Up to 16 foils were welded with optimized welding parameters to ensure substrate fracture regardless of the number of foils in the stack. The results of electrical resistance measurements and tensile tests depending on the number of welded foils, as well as an overview of the welding parameters, are presented in Figure 11.

The fracture forces increase with the number of foils in the stack. The maximum fracture force was recorded when 12 foils were welded. The continuous increase is mainly due to the larger number of foils welded and thus the overall higher load-bearing capacity of the foils. The fractures occur primarily in the outer area of the weld zone, where the material has thinned due to the welding process. For this reason, the strength does not increase linearly with the number of foils. For the 16-layer specimens, the fracture force decreases significantly while having an adhesive fracture in the specimens. Welding more than 16 foils is not attainable due to the weak adhesion between the arrester tab and the foil stack. This corresponds with the energy input required to produce the welds. From the welding parameters, it can be seen that the required energy input to achieve sufficient welds increases with the number of foils. However, if the number of foils is too high, a further increase in energy input cannot create high-strength welds as the adhesion between the layers is too low to create joints. Instead, the high energy input leads to a strong sticking to the anvil.

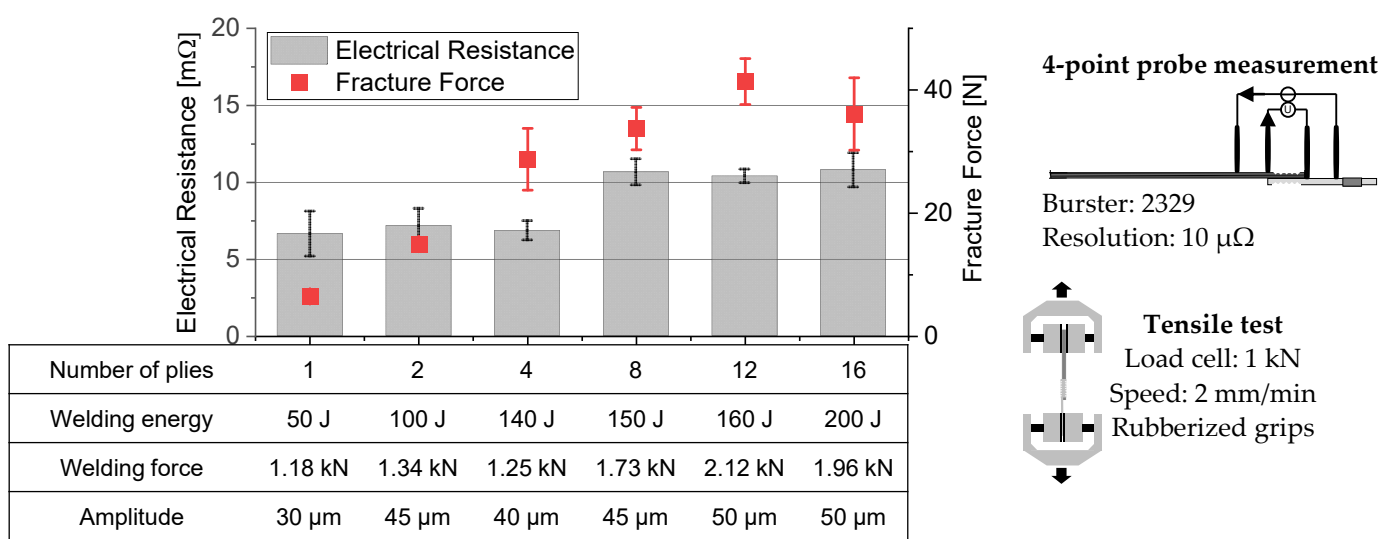
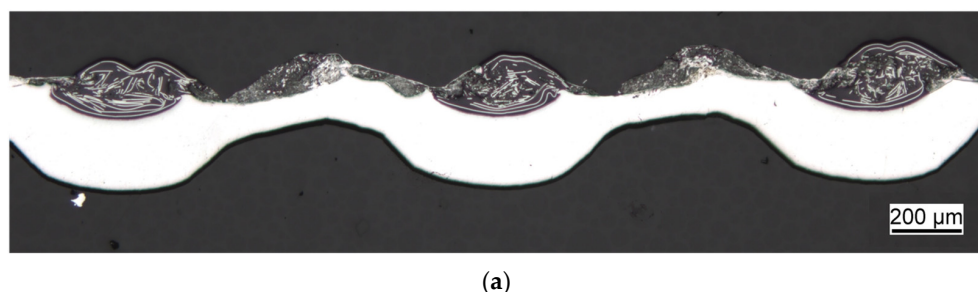


Figure 11. Impact of the number of foils welded with optimized parameters on the electrical resistance and fracture force of the welds.

The measurements of the electrical resistances of the respective welded joints can be divided into two ranges. One range is between one and four Al@PET foil sheets, where the electrical resistance is relatively constant at about 7 mΩ. The other range, with an electrical resistance of about 11 mΩ, is between 8 and 16 welded sheets. The explanation for this is that, in the welds with up to four foils, the electrical paths are short, but the thermoplastic is not yet fully plasticized. Therefore, the electrical resistance is not significantly lower in the one-foil weld than in the four-foil weld. In welds with 8 or more foils, sufficient thermal energy is introduced to melt the PET. Simultaneously, however, the pressure generated during the process also pushes the PET out of the area of the horn tips. As a result, the length of the conduction paths does not change, and since the ratio of aluminum to PET remains the same, the electrical resistance is similar. Thus, the resistance depends only on the length of the conduction paths and whether the PET actually melts completely and the metallization fragments enter the polymer. The fragments are thereby small particles from the former aluminum coating that remain in the PET after the welding process.

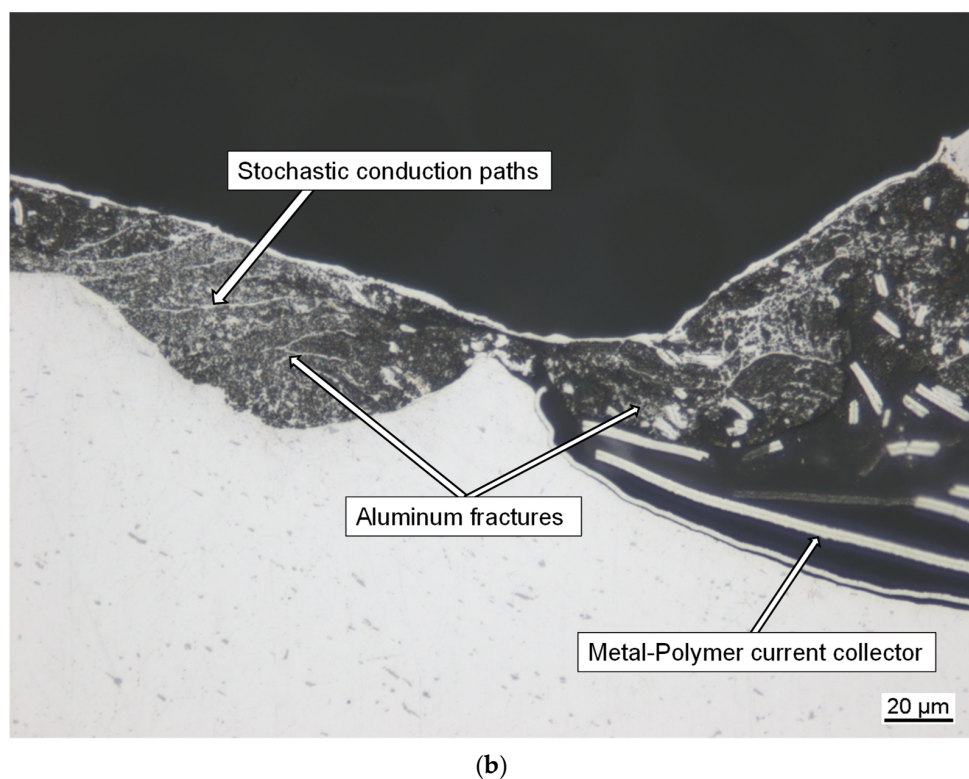
The cross-section of an ultrasonically welded joint with 16 foils proves that the foil structure is destroyed and stochastically distributed conduction paths are formed, which are responsible for the electrical contact (Figure 12).

A change in electrical resistance that could have resulted from the altered fracture pattern is not discernible in the resistance measurements for 16 sheets. Nevertheless, the weld resistance is at least an order of magnitude higher than that of ultrasonically welded joints with conventional aluminum or copper foil [38].



(a)

Figure 12. Cont.



(b)

Figure 12. Microscopic image of a cross-section from an ultrasonically welded joint with 16 foils of aluminum-coated PET foil (a) with $100\times$ and (b) $1000\times$ magnification.

3.2. Laser Beam Welding

Laser beam welding tests were conducted using the Al@PET foil (V1). It is important to note that no welding was achieved. Light microscope images reveal a strong formation of soot on the foils and a retraction of the foils from the laser beam area. This is evidenced by wrinkles at the edges. Additionally, the width of the cut caused by the foil retraction is approximately $100\text{ }\mu\text{m}$, which is considerably larger than the laser beam spot diameter ($70\text{ }\mu\text{m}$) (see Figure 13). Furthermore, the heat input from the laser beam results in a large heat-affected zone, distinguishable due to the wrinkling and retraction of the foil in this area. This begins to occur at temperatures around $110\text{ }^{\circ}\text{C}$, at which point the foil starts to shrink. In this regard, the metal–polymer foil fulfills its function of retracting at elevated temperatures, which has a detrimental effect during fusion welding and thus renders it unsuitable for laser welding.

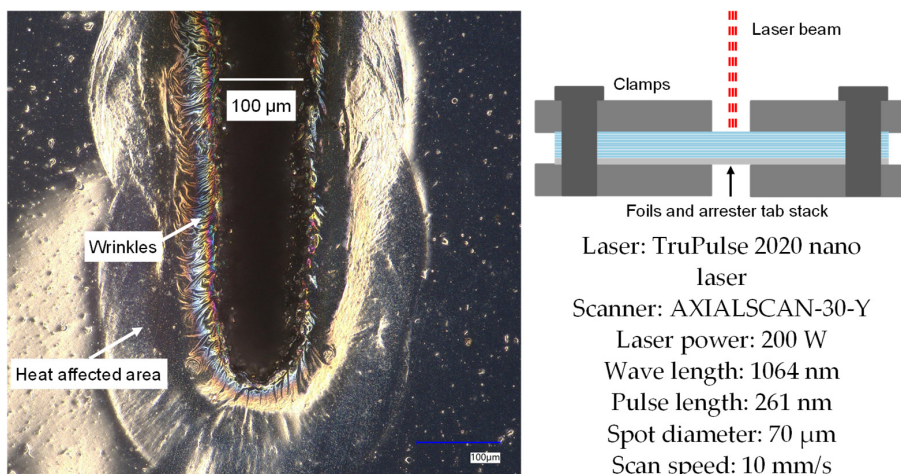


Figure 13. Microscopic image of a foil after the welding experiment.

3.3. Mechanical Contacting as an Alternative Joining Process

Mechanical contacting by clamping the foils between electrically conductive interlayers could be an alternative to the welding process, despite the increased process effort. At the same time, this method could be independent of the number of foils to be contacted and thus not limited in this respect. In addition, the specimens can be produced without visible damage to the foils (as illustrated in Figure 14a).

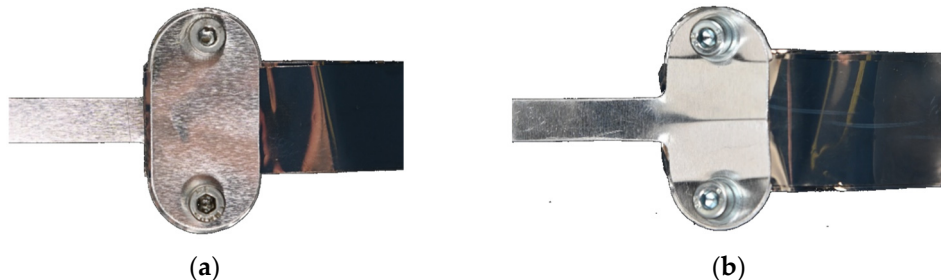


Figure 14. (a) Specimen manufactured by mechanical clamping and (b) same specimen tested.

The subsequent tensile tests were performed on specimens with 15, 20, and 30 foils made of material V1. Substrate fracture occurs due to high plastic strains in the foils. The bottom tabs also deform (see Figure 14b).

The achieved strength reaches up to 240 N, six times the fracture strength of the ultrasonically welded joint. This is enabled by the integrity of the foils during the joining process. This is not given with ultrasonic welding. The fracture strength is highest for 15 sheets and about 30% lower for 20 and 30 sheets. This may be due to the slightly eccentric force application. However, there is a large scatter in the tensile tests (see Figure 15).

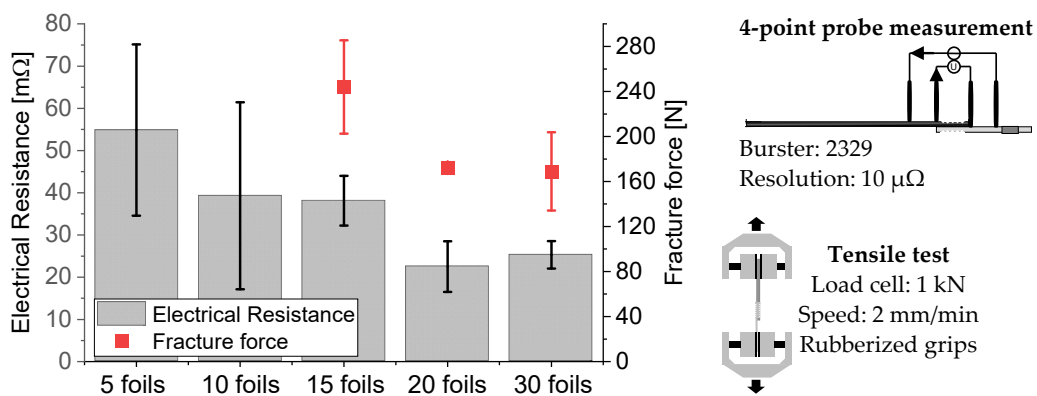


Figure 15. Properties of mechanically clamped metal–polymer foil stacks.

In the four-point probe measurements, the resistance drops from 55 mΩ when contacting five foils to as low as 25 mΩ when contacting 20 foils. In addition, the high standard deviation at five and ten foils decreases. This can be attributed to the increasing thickness of the foil stack, which results in a higher surface pressure caused by the design of the clamps. Between 20 and 30 sheets, there are no significant differences in electrical resistance.

4. Discussion

To be suitable for contacting, a current collector must first be joinable or weldable. This was achieved with two of the three joining processes. Laser welding proved to be unsuitable due to the high heat input that melted the thermoplastic substrate and caused the foil to withdraw, preventing the formation of a viable joint. This circumstance rules out fusion welding processes for contacting, as they typically involve high temperatures that could damage the polymer substrate.

Ultrasonic welding was able to produce welds of sufficient quality for laboratory cells. However, it should be noted that the process window for ultrasonic welding with the metal–polymer current collector is significantly narrower than for comparable welds with conventional aluminum or copper foil, as adhesive fractures, cracks, and anvil sticking occur earlier compared to full metal foils. The melting of the polymer substrate is likely the cause of this. The molten polymer also ensures an adhesive attachment of the foils to the metallic arrester tab. Thereby, the polymer, especially PET, forms only low adhesion to the tab without prior surface pretreatment. Therefore, it is expected that the adhesion will not significantly change with the number of foils to be welded or the associated welding parameters. Furthermore, the molten polymer also adheres to the anvil, causing strong sticking. This results in a significantly reduced process window compared to metal foil welds and, in the limit case, lead to adhesive fractures during tensile testing.

Thus, the process is limited for large-scale applications. This is due to two main reasons: First, it was not possible to weld more than 16 current collectors. This falls significantly short of the requirements for industrial applications. Second, both the mechanical strength and electrical resistance of the weld tend to increase with the number of welded foils.

The tensile strength of the welded joints was adequate, but it did not increase proportionally to the number of foils. The molten polymer displacement during the ultrasonic welding process significantly reduces the thickness in the areas of the weld spots, causing the polymer to lose its rigid alignment and resulting in a loss of strength. Additionally, the foils may be partially perforated or torn, which promotes crack propagation. In combination, these factors lead to a substantial decrease in the mechanical load-bearing capacity.

The most important property is probably the weld resistance of the joint. The weld resistances measured were significantly higher than those of metal foil welds, ranging from five to twelve milliohm. The electrical contacting is possible by enabling electrical conductivity over multiple foil layers through the fragments in the molten polymer. The fine distribution and arrangement of these fragments ensure reproducible measurement results. Correspondingly, the high number of contact resistances between the fragments in the polymer increases the electrical resistance compared to a homogeneous coating, limiting the achievable electrical conductivity of the welds. Thereby, the weld behaves like a polymer with electrically conductive fillers. However, the filling effect is restricted in terms of the electrical resistance [39]. The achieved weld resistance would result in high power losses during fast charging and discharging, causing the cell to heat up considerably. Thereby, the biggest lever for reducing electrical resistance is to increase the thickness of the metallization. This improves the density and size of the electrical conduction paths following the welding process. However, achieving a resistance of less than one milliohm would likely require several micrometers of coating thickness. This is not feasible from either a process or economic perspective, as even depositing a coating thickness of one micrometer generates high temperatures during electron beam evaporation, necessitating specialized cooling. A further thickening of the coating would only be possible if the foils were coated in several passes. This would significantly increase costs, making metallic aluminum and copper current collectors more attractive from an economic standpoint. This also holds true for other coating processes such as electrochemical deposition.

A switch to other, more temperature-stable polymer substrates could therefore be advantageous. This would allow for a corresponding reduction in substrate thickness. However, even the use of a different polymer substrate (6 µm PEN instead of 12 µm PET) has not shown any significant impact on the properties of the welded joints for the copper-coated metal–polymer current collectors. Nevertheless, it is important to note that the PEN substrate is both thinner and more temperature-resistant than the PET substrate. These properties may counteract each other, as the length of the conduction path and the melting of the thermoplastics are two factors that influence the electrical resistance of the weld. Therefore, it is not possible to determine whether a PEN substrate of the same thickness would behave identically to the PET substrate.

Based on these findings, it can be stated that the potential for contacting metal–polymer collectors using ultrasonic welding is limited by both the high electrical resistance of the weld and the restricted number of weldable foils. Furthermore, the joint's resistance to aging under the extreme conditions within a cell is not certain. The differing thermal expansion coefficients of aluminum and PET can induce critical mechanical stresses within the cell. This expansion can also disrupt electrically conductive paths, thereby increasing the electrical resistance. These factors, along with the chemical exposure of PET to the electrolyte, could negate the benefits of metal–polymer current collectors [40,41].

The alternative contacting process by clamping is presumed to be independent of the number of joinable foils. In this method, the foils are contacted on both sides over a large area without causing any damage. Consequently, the ability to join is assured. Electrical conductivity is achieved through the surface pressure between the current collectors and the aluminum contacting aids. These aids then conduct the electrical current via the screws to the bottom arrester tab. However, the electrical resistance remains unsatisfactory and is the limiting factor of this process. In some instances, the electrical resistance was several times higher than that of ultrasonically welded joints. This restricts the application of this method within battery cells. Thereby, the resistance steadily decreased up to the 20-foil specimens and then leveled off. At this point, a uniform surface pressure was achieved, which did not further increase with the number of foils. Therefore, from 20 foils onward, the electrical resistance is independent of the metal–polymer foils examined (see Table 2).

Table 2. Evaluation of the investigated joining methods with regard to their suitability for contacting battery cells.

Process	Joinability/Weldability	Mechanical Load Bearing Capacity	Electrical Resistance
US welding	✓	O	O
Laser beam welding	X	-	-
Clamping	✓	+	O/-

The electrical resistance can be further reduced by increasing the surface pressure and eliminating unnecessary contact resistances, such as between the contacting aid and screw, and between the screw and arrester tab, by employing alternative joining methods. Indeed, an adaptation of the design is necessary for use in cells. The positioning of the foils and the preparation of the clamped specimen were complex. Additionally, the use of steel screws in a cell would also be unsuitable for electrochemical reasons. Nickel or aluminum would have to be used on the cathode side, which would likely require a modified design. Therefore, a more effective approach might be to substitute the screws and utilize other joining methods, such as ultrasonic welding or laser beam welding, for contacting the aluminum aids and arrester tabs. These methods do not require any supplementary material and, consequently, do not add additional mass.

Nevertheless, the contact resistance of the current collectors cannot be reduced at will and will remain above one milliohm, even when applying the highest surface pressure. Conversely, surface pretreatment could significantly reduce the contact resistance [42], but would be a further inhibition threshold for the use of metal–polymer current collectors due to the fast cycle times in battery cell production.

The design used here achieved high fracture strength in the tensile tests. The slight decrease in fracture force for specimens with 20 and 30 foils is primarily due to the challenges of positioning the foils, resulting in an uneven stress distribution within the specimen. Nevertheless, the mechanical strength remains adequate. It is anticipated that the environmental conditions within the cell will not significantly alter the joint properties when clamping is employed.

Hence, compared to the ultrasonic welding process, the clamping process offers advantages in terms of the number of foils that can be joined and mechanical strength.

However, in all other aspects (electrical resistance, process implementation, and effort), ultrasonic welding is more suitable.

5. Conclusions

It has been demonstrated that ultrasonic welding and mechanical clamping can be employed to join the investigated foils. In both cases, reproducible results have been achieved in terms of mechanical strength and electrical resistance.

However, the joining mechanisms differ fundamentally. Ultrasonic welding involves melting the thermoplastic core, leaving small fragments of the metallization embedded in the PET that facilitate electrical conductivity. The coating thickness has proven to be a significant influencing factor in this process. But, the melting process severely limits the number of weldable foils due to sticking to the tools. Mechanical clamping, on the other hand, is independent of this limitation. Here, the electrical resistance stems from the contact resistances within the joint.

In both cases, the electrical resistance is in the range of several milliohms. Reducing it to the level of intermetallic joints will not be feasible. Therefore, while both processes allow for the contacting of laboratory cells, they will lead to substantial power and energy losses at high currents. Ultrasonic welding is already reaching its process limits in this regard. Clamping, on the other hand, still offers the possibility of reducing the electrical resistance, which would be necessary for industrial applications. Nevertheless, it remains questionable whether such a process can be integrated into the existing process chain for battery cell production. Laser beam welding was not suitable due to the high energy input required.

Hence, further research must focus on developing new and adapted processes. This includes multi-stage processes, such as pre-steps to ultrasonic welding that enable the formation of electrical conduction paths through the metal–polymer current collectors.

Author Contributions: Conceptualization, H.G. and M.M.; methodology, H.G. and T.K.; testing and validation, H.G. and T.K.; formal analysis, H.G.; investigation, H.G.; writing—original draft preparation, H.G.; writing—review and editing, H.G., M.M., M.W.K., T.K. and K.D.; visualization, H.G. and M.M.; supervision, M.W.K. and K.D.; project administration, M.M.; funding acquisition, M.W.K. and K.D. All authors have read and agreed to the published version of the manuscript.

Funding: This research was funded by the German Federal Ministry of Education and Research under grant no. 03XP0408E. The author is responsible for the content of this publication.

Data Availability Statement: The data presented in this study are available on request from the corresponding author.

Acknowledgments: The researchers would like to thank Fraunhofer FEP for providing the materials.

Conflicts of Interest: The authors declare no conflict of interest.

References

1. Zhu, P.; Gastol, D.; Marshall, J.; Sommerville, R.; Goodship, V.; Kendrick, E. A review of current collectors for lithium-ion batteries. *J. Power Sources* **2021**, *485*, 229321. [[CrossRef](#)]
2. Grabmann, S.; Tomcic, L.; Zaeh, M.F. Laser beam welding of copper foil stacks using a green high power disk laser. *Procedia CIRP* **2020**, *94*, 582–586. [[CrossRef](#)]
3. Korthauer, R. *Lithium-Ion Batteries: Basics and Applications*; Springer: Berlin/Heidelberg, Germany, 2018; ISBN 978-3-662-53069-6.
4. Korthauer, R. *Handbuch Lithium-Ionen-Batterien*; Springer: Berlin/Heidelberg, Germany, 2013; ISBN 978-3-642-30652-5.
5. Sigl, M.E.; Grabmann, S.; Kick, L.-F.; Zens, A.; Hartl, R.; Zaeh, M.F. Cell-Internal Contacting of Prismatic Lithium-Ion Batteries Using Micro-Friction Stir Spot Welding. *Batteries* **2022**, *8*, 174. [[CrossRef](#)]
6. Grabmann, S.; Mayr, L.; Kick, M.K.; Zaeh, M.F. Enhancing laser-based contacting of aluminum current collector foils for the production of lithium-ion batteries using a nanosecond pulsed fiber laser. *Procedia CIRP* **2022**, *111*, 778–783. [[CrossRef](#)]
7. Grabmann, S.; Kick, M.K.; Geiger, C.; Harst, F.; Bachmann, A.; Zaeh, M.F. Toward the flexible production of large-format lithium-ion batteries using laser-based cell-internal contacting. *J. Laser Appl.* **2022**, *34*, 42017. [[CrossRef](#)]
8. Arimoto, K.; Sasaki, T.; Doi, Y.; Kim, T. Ultrasonic Bonding of Multi-Layered Foil Using a Cylindrical Surface Tool. *Metals* **2019**, *9*, 505. [[CrossRef](#)]
9. Wassiliadis, N.; Ank, M.; Wildfeuer, L.; Kick, M.K.; Lienkamp, M. Experimental investigation of the influence of electrical contact resistance on lithium-ion battery testing for fast-charge applications. *Appl. Energy* **2021**, *295*, 117064. [[CrossRef](#)]

10. Shin, S.; Nam, S.; Yu, J.; Park, J.; Kim, D. Ultrasonic Metal Welding of Multilayered Copper Foils to Nickel-Plated Copper Sheet in Lithium-Ion Battery Cell. *Metals* **2021**, *11*, 1195. [[CrossRef](#)]
11. Brand, M.J.; Schmidt, P.A.; Zaehe, M.F.; Jossen, A. Welding techniques for battery cells and resulting electrical contact resistances. *J. Energy Storage* **2015**, *1*, 7–14. [[CrossRef](#)]
12. Pham, M.T.; Darst, J.J.; Walker, W.Q.; Heenan, T.M.; Patel, D.; Iacoviello, F.; Rack, A.; Olbinado, M.P.; Hinds, G.; Brett, D.J.; et al. Prevention of lithium-ion battery thermal runaway using polymer-substrate current collectors. *Cell Rep. Phys. Sci.* **2021**, *2*, 100360. [[CrossRef](#)]
13. Choudhury, R.; Wild, J.; Yang, Y. Engineering current collectors for batteries with high specific energy. *Joule* **2021**, *5*, 1301–1305. [[CrossRef](#)]
14. Luber, C.; Scheffel, B.; Saager, S.; Straach, S.; Schiller, N. Lithium-Ionen-Batterien: Potenzial von Vakuumdünnschichtprozessen in der Herstellung. *Vak. Forsch. Und Prax.* **2018**, *30*, 39–45. [[CrossRef](#)]
15. Liang, C.; Huang, H.; Huang, Q. Current Collector, Electrode Plate Including the Same and Battery. European Patent EP3509145_B1, 26 July 2023.
16. Ye, Y.; Chou, L.-Y.; Liu, Y.; Wang, H.; Lee, H.K.; Huang, W.; Wan, J.; Liu, K.; Zhou, G.; Yang, Y.; et al. Ultralight and fire-extinguishing current collectors for high-energy and high-safety lithium-ion batteries. *Nat. Energy* **2020**, *5*, 786–793. [[CrossRef](#)]
17. Darcy, E. Metallized Plastic Current Collectors. In Proceedings of the Advanced Automotive Battery Conference, San Diego, CA, USA, 24–27 June 2019.
18. Morin, B. Lithium Energy Storage Device with Internal Fuse. U.S. Patent 10,854,868,B2, 1 December 2020.
19. Xiang, L.; Xing, C.; Wang, P.; Cai, R. Electrode Member, Electrode Assembly and Rechargeable Battery. European Patent EP3490033_B1, 4 March 2020.
20. Zhang, Z.; Song, Y.; Zhang, B.; Wang, L.; He, X. Metallized Plastic Foils: A Promising Solution for High-Energy Lithium-Ion Battery Current Collectors. *Adv. Energy Mater.* **2023**, *13*, 2302134. [[CrossRef](#)]
21. Zhang, Z.; Xue, Q.; Jiang, M.; Li, J.; Li, W. Secondary Battery and Electrode Plate. European Patent EP3595044_B1, 28 July 2021.
22. Zhou, Y.; Xue, Q.; Zhang, Z.; Jiang, M.; Li, J.; Li, W.; Wang, L. Secondary Battery and Electrode Plate Thereof. European Patent EP3588620_A1, 31 August 2022.
23. Zhou, Y.; Xue, Q.; Zhang, Z.; Jiang, M.; Li, J.; Li, W.; Wang, L. Secondary Battery and Electrode Plate Thereof. European Patent EP3588619_B1, 3 March 2021.
24. Wu, C.; Lin, J.; Zhou, L.; Zhang, X.; Li, K.; Wu, Z. Processing Apparatus for Secondary Battery Current Collector. European Patent EP3539772_A1, 18 September 2019.
25. Gisario, A.; Aversa, C.; Barletta, M.; Natali, S.; Veniali, F. Laser transmission welding of aluminum film coated with heat sealable co-polyester resin with polypropylene films for applications in food and drug packaging. *Int. J. Adv. Manuf. Technol.* **2022**, *120*, 2291–2309. [[CrossRef](#)]
26. Pagano, N.; Campana, G.; Fiorini, M.; Morelli, R. Laser transmission welding of polylactide to aluminium thin films for applications in the food-packaging industry. *Opt. Laser Technol.* **2017**, *91*, 80–84. [[CrossRef](#)]
27. Fromme, N.P.; Li, Y.; Camenzind, M.; Toncelli, C.; Rossi, R.M. Metal-Textile Laser Welding for Wearable Sensors Applications. *Adv. Electron. Mater.* **2021**, *7*, 2001238. [[CrossRef](#)]
28. Melentiev, R.; Yudhanto, A.; Tao, R.; Vuchkov, T.; Lubineau, G. Metallization of polymers and composites: State-of-the-art approaches. *Mater. Des.* **2022**, *221*, 110958. [[CrossRef](#)]
29. Amancio Filho, S.D.T.; Feistauer, E.E.; Dos Santos, J.F. Method for Connecting a Surface-Structured Workpiece and a Plastic Workpiece. U.S. Patent 9,925,717, 27 March 2018.
30. Feistauer, E.E.; Santos, J.F.; Amancio-Filho, S.T. A review on direct assembly of through-the-thickness reinforced metal-polymer composite hybrid structures. *Polym. Eng. Sci.* **2018**, *2019*, 661–674. [[CrossRef](#)]
31. Palkowski, H.; Giese, P.; Wesling, P.; Lange, G.; Spieler, S.; Goellner, J. Neuartige Sandwichverbunde—Herstellung, Umformverhalten, Fügen und Korrosionsverhalten. *Mat.-Wiss. U. Werkst.* **2006**, *37*, 605–612. [[CrossRef](#)]
32. Murzin, S.P.; Palkowski, H.; Melnikov, A.A.; Blokhin, M.V. Laser Welding of Metal-Polymer-Metal Sandwich Panels. *Metals* **2022**, *12*, 256. [[CrossRef](#)]
33. Balz, I.; Rosenthal, E.; Reimer, A.; Turiaux, M.; Schiebahn, A.; Reisgen, U. Analysis of the thermo-mechanical mechanism during ultrasonic welding of battery tabs using high-speed image capturing. *Weld World* **2019**, *63*, 1573–1582. [[CrossRef](#)]
34. Lu, Y.; Song, H.; Taber, G.A.; Foster, D.R.; Daehn, G.S.; Zhang, W. In-situ measurement of relative motion during ultrasonic spot welding of aluminum alloy using Photonic Doppler Velocimetry. *J. Mater. Process. Technol.* **2016**, *231*, 431–440. [[CrossRef](#)]
35. DiFinizio, T. Ultrasonic intelligence. *Wire Cable Technol. Int.* **2005**, *33*, 88–90.
36. Balz, I. Prozessanalyse der Thermomechanischen Vorgänge während der Verbindungsbildung beim Metall-Ultraschallschweißen. Ph.D. Dissertation, RWTH Aachen University, Aachen, Germany, 2020.
37. Müller, F.W.; Schiebahn, A.; Reisgen, U. Quality prediction of disturbed ultrasonic metal welds. *J. Adv. Join. Process.* **2022**, *5*, 100086. [[CrossRef](#)]
38. Shin, H.-S.; de Leon, M. Mechanical performance and electrical resistance of ultrasonic welded multiple Cu-Al layers. *J. Mater. Process. Technol.* **2017**, *241*, 141–153. [[CrossRef](#)]
39. Sumita, M.; Sakata, K.; Asai, S.; Miyasaka, K.; Nakagawa, H. Dispersion of fillers and the electrical conductivity of polymer blends filled with carbon black. *Polym. Bull.* **1991**, *25*, 265–271. [[CrossRef](#)]

40. Adamson, A.; Tuul, K.; Bötticher, T.; Azam, S.; Garayt, M.D.L.; Metzger, M. Improving lithium-ion cells by replacing polyethylene terephthalate jellyroll tape. *Nat. Mater.* **2023**, *22*, 1380–1386. [[CrossRef](#)] [[PubMed](#)]
41. Buechele, S.; Logan, E.; Boulanger, T.; Azam, S.; Eldesoky, A.; Song, W.; Johnson, M.B.; Metzger, M. Reversible Self-discharge of LFP/Graphite and NMC811/Graphite Cells Originating from Redox Shuttle Generation. *J. Electrochem. Soc.* **2023**, *170*, 10518. [[CrossRef](#)]
42. Crinon, E.; Evans, J.T. The effect of surface roughness, oxide film thickness and interfacial sliding on the electrical contact resistance of aluminium. *Mater. Sci. Eng. A* **1997**, *242*, 121–128. [[CrossRef](#)]

Disclaimer/Publisher's Note: The statements, opinions and data contained in all publications are solely those of the individual author(s) and contributor(s) and not of MDPI and/or the editor(s). MDPI and/or the editor(s) disclaim responsibility for any injury to people or property resulting from any ideas, methods, instructions or products referred to in the content.